JOURNAL OF APPLIED ELECTROCHEMISTRY 19 (1989) 617–629

Potential drops due to an attached bubble on a gas-evolving electrode*

C. GABRIELLI, F. HUET, M. KEDDAM, A. MACIAS‡, A. SAHAR

LP15 du CNRS, Physique des Liquides et Electrochimie, Laboratoire de l'Université Pierre et Marie Curie, Tour 22, 4 place Jussieu, 75252 Paris Cedex 05, France

Received 28 September 1988; revised 13 February 1989

It is shown how the various components of the overpotential due to an attached bubble on an electrode can be separated and estimated. By considering the resistance increments due to the presence on the electrode surface of a bubble, obtained from impedance measurements, it is possible to determine the predominant potential distribution which controls the gas evolution. A relationship between the measured overpotential and the diameter of the bubble is established. The time evolution of the overpotential due to a growing bubble is modelled in the case of the limitation of the bubble growth by dissolved gas diffusion in the solution. In agreement with previous experimental results a linear time variation is found.

Nomenclature

b_b, b_f	Tafel coefficients (V^{-1}) Equation A7
δc	difference between the supersaturation and saturation concentrations ($mol\,m^{-3}$)
C	electrode double layer capacity (F)
C_0	electrode double layer capacity per surface unit ($F\,m^{-2}$)
C_A, C_B	concentrations of species A and B in the redox system ($mol\,m^{-3}$)
d_b	diameter of a bubble or a sphere on the electrode (m)
d_e	diameter of the disc electrode (m)
D	diffusion coefficient of the dissolved gas ($m^2\,s^{-1}$)
E	electrode potential (V)
E_z	zero-charge potential of the electrode (V)
F	Faraday constant, $= 96487\,C\,mol^{-1}$
I	electrolysis current (A)
I_F	faradaic current (A)
k_b, k_f	heterogeneous rate constants of the redox reaction ($m\,s^{-1}$)
k_1	slope of $\Delta V/t$ curve ($V\,s^{-1}$), Equation 5
k_2	slope of $\Delta V/t^{2/3}$ curve ($V\,s^{-2/3}$), Equation 5
K	Henry coefficient, Equation 1
n	number of the electrons involved in the reaction to form one molecule of the dissolved gas
Q	electrical charge of the electrode double layer (C)
r_b	radius of a bubble or of a sphere on the electrode (m)
R_e	electrolyte resistance (Ω)
R_{e0}	electrolyte resistance for an electrode of 1 m in diameter (Ωm), Equation 32
R_p	polarization resistance (Ω)
R_{p0}	polarization resistance per surface unit ($\Omega\,m^{-2}$)
R_t	charge-transfer resistance (Ω)
s	relative rate of variation of the electrode active surface due to a growing bubble (s^{-1})
S	disk electrode surface (m^2)
ΔS_e, ΔS_p	equivalent screened surfaces by a bubble or a sphere given by R_e and R_p changes (m^2), Equations 18 and 29
t	time (s)
V	potential difference between the working and the reference electrodes (V)
V_0	gas molar volume: $24.5 \times 10^{-3}\,m^3$ at 298 K
ΔV	total overpotential increment due to a bubble or a sphere (V)
ΔV_a, ΔV_{ohm}	activation and ohmic overpotential increments due to a bubble or a sphere (V)

Greek characters

α	slope of $\log \Delta V/\log I$ curve, Equation 11
α_e, α_p	dimensionless parameters in Equations 27 and 30
β	dimensionless coefficient in Scriven law, Equation 2
η_t	total overpotential (V)
η_a, η_c, η_{ohm}	spatial averages of the activation, concentration and ohmic overpotentials over the electrode surface (V)
ϱ	electrolyte density ($kg\,m^{-3}$)

Subscript

i	in the absence of the growing bubble

* Paper presented at the 2nd International Symposium on Electrolytic Bubbles organized jointly by the Electrochemical Technology Group of the Society of Chemical Industry and the Electrochemistry Group of the Royal Society of Chemistry and held at Imperial College, London, 31st May and 1st June 1988.

‡ On leave from Instituto Eduardo Torroja (C.S.I.C.), c/Serrano Galvache, Madrid 28033, Spain.

0021-891X/89 $03.00 + .12

1. Introduction

Gas evolution occurs on an electrode through several phenomena. The gas produced in molecular form by electrochemical reactions on the electrode dissolves in the electrolyte and is transported by convection and diffusion towards the bulk of the solution. A molecular gas supersaturation in the vicinity of the electrode and some active sites on the surface lead to bubble nucleation [1–4]. The growth of the bubbles develops in two or three steps depending on the size of the electrode.

In the first step of the growth, from a bubble nucleus of the critical size, it has been shown, from Rayleigh's work [5] that the radius, $r_b(t)$, of the bubble changes with time, t, as

$$r_b(t) = \left(\frac{2K\delta c}{3\varrho}\right)^{1/2} t \qquad (1)$$

where K is the Henry coefficient, δc is the difference between the supersaturation and saturation concentrations and ϱ is the electrolyte density [6, 7]. The second step has been studied by Scriven [8]; he has shown that when the bubble growth is limited by the diffusion of the dissolved gas, one has

$$r_b(t) = 2\beta(Dt)^{1/2} \qquad (2)$$

where D is the diffusion coefficient of the dissolved molecular gas and β is a current-dependent growth coefficient. The third step is limited by the kinetics of the production of the dissolved gas [9, 10]. When the bubble is larger than the electrode, it is assumed that the gas produced in molecular form is all transformed to the gaseous form which increases the bubble size. In this case

$$r_b(t) = \left(\frac{3V_0It}{4\pi nF}\right)^{1/3} \qquad (3)$$

where V_0 is the molar volume of the gas, I the electrolysis current, n the number of electrons involved in the electrochemical reaction and F the Faraday constant. Brandon and Kelsall [7] have verified the validity of Equations 1–3 in experiments carried out on microelectrodes of diameters ranging from 10 to 500 μm.

The last stage of the bubble evolution, i.e. its detachment from the surface, occurs when the balance between the forces which tend to maintain it on the electrode and the forces which tend to release it is broken [9]. These various forces include the weight of the bubble, the buoyancy, the superficial tension, the pressure, the inertia and the electrostatic forces [7].

The electrochemical reaction mechanisms which lead to the production of the gas in molecular form have been investigated [11]. However this paper deals with the overpotentials arising from the presence of a bubble on the electrode surface.

Information on the fundamental aspects of the potential drops related to a gas-evolving electrode have been provided by Leistra and Sides [12] who have estimated the various terms of the overpotential (ohmic η_{ohm}, activation η_a, and concentration η_c). Dukovic and Tobias [13] have carried out a numerical calculation of the total overpotential on an infinite electrode by taking into account the primary, secondary and tertiary potential distributions. They have shown that the total overpotential can be expressed by

$$\eta_t = \eta_{ohm} + \eta_a + \eta_c \qquad (4)$$

In this paper the various components of the total overpotential will be experimentally estimated. In particular these terms will be related to the sizes of the bubble and the electrode. This calibration will allow, in a subsequent paper [14], a quantification of the bubble mean size and the evolved gas volume (evolution efficiency) from the power spectral density of the voltage fluctuations measured on a gas-evolving electrode [15].

In a first step, the correlation between the time evolution of the radius of a growing bubble and the induced overpotential will be investigated on a microelectrode. In a second step, the various components of the steady state overpotential will be separated in the case of a sphere, simulating a 'frozen' bubble, placed on the electrode surface. In a third step, a model of the dynamic behaviour of the potential drops related to the bubble growth will be derived.

2. Experimental details

Two types of experiment were carried out: first a measurement of the time evolution of the radius of the growing bubble and then measurements of electrical quantities (steady state voltages and impedance).

The measurements were performed in a cylindrical cell where the working electrode was located close to an optical window made through the side wall of the cell. This window was used for taking photographs or for observing the electrode by means of a binocular microscope. The electrode faced upwards in order to facilitate the release of the gaseous bubbles or the laying of a glass sphere on the surface. The electrode was a disc of various diameters (that of 100 μm diameter being termed a microelectrode) insulated in glass. The electrode surface was first polished with emery paper (grade 1200) and then with alumina powder (3000 Å). The reference electrode was of the saturated calomel type in NaOH medium and of the saturated sulphate type in a sulphuric medium. The counter electrode was a platinum grid. In all the experiments the current was controlled in order to observe only the overpotential due to the bubble growth or to the presence of the sphere.

2.1. *Measurement of the electrical quantities*

The electrical signals (current, potential) were amplified and cleared for their d.c. components. A monitoring oscilloscope allowed the current to be kept constant during the bubble growth and detachment.

In the microelectrode experiment the time evolution of the overpotential increment, $\Delta V(t)$, due to the

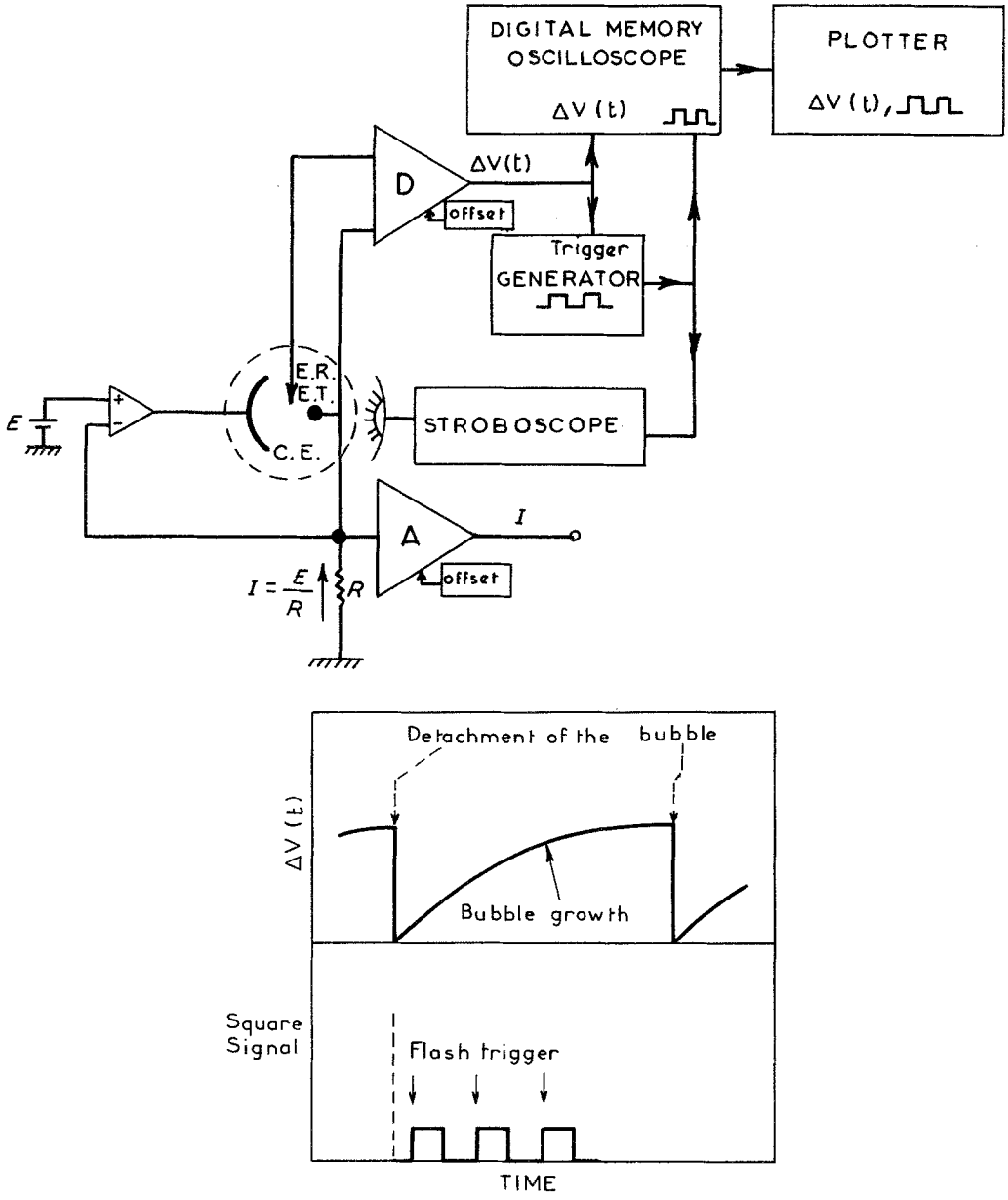

Fig. 1. (a) Experimental arrangement for the simultaneous measurement of the overpotential increment $\Delta V(t)$ and the bubble radius by means of a stroboscope. (b) Signals recorded on the digital memory oscilloscope (overpotential increment $\Delta V(t)$ and instants of the stroboscope flashes).

bubble growth was recorded by using a digital memory oscilloscope (two channel Gould OS4200) which was also used to synchronize the stroboscope triggering used to measure the bubble radius (Fig. 1a). At the end of the acquisition the signal $\Delta V(t)$ was drawn on a plotting table.

By superimposing white noise to the current as a perturbing signal and comparing it with a Fourier analyser to the system response in voltage, the impedance was measured [16].

2.2. *Measurement of the time evolution of the bubble radius*

The detachment of the bubble from the electrode surface induces a steep jump of the overpotential (Fig. 2) which allows a programmable signal generator (Wavetek 275), which delivers a periodical square signal, to be triggered in order to control the stroboscope. The latter generated very short flashes (a few μs) which lit the electrode at successive instants of the bubble growth. The periodical square signal was also stored in the second channel of the oscilloscope in order to mark the triggering times of the flashes (Fig. 1b).

The photograph was taken by using a camera with a bellows which gave an enlargement of 5 on the negative. By keeping the camera shutter open ('B' position of the shutter dial) successive pictures of the bubble at periodical instants were produced on the film. Hence a succession of pictures of the bubble taken at constant time intervals was obtained on the same photograph, from which the time evolution of the bubble radius could be measured (Fig. 3). As the sequence nucleation–growth–detachment of the bubble was periodic on the microelectrode, by varying the fre-

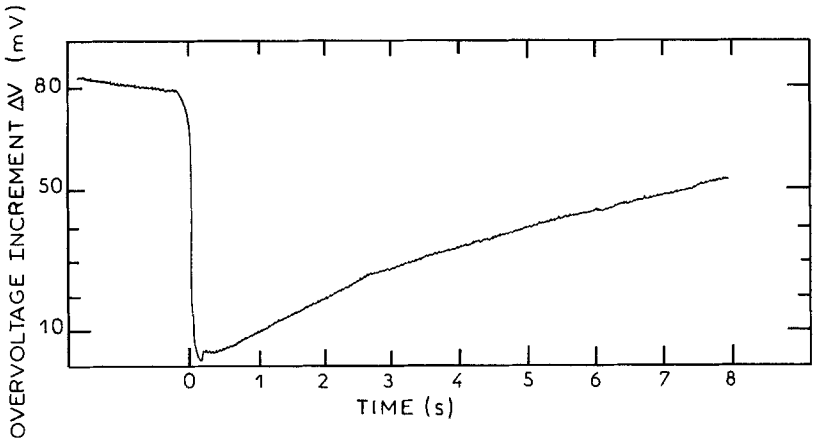

Fig. 2. Time evolution of the overpotential increment $\Delta V(t)$ due to the growth of an oxygen bubble on a microelectrode (d_e = 100 μm, I = 67 μA, 1 M NaOH).

quency and the number of cycles of the square signal delivered by the generator, the whole transient could be explored.

Two limitations have appeared. Firstly the horizontality of the electrode surface influenced the shape of the $\Delta V(t)$ transient a great deal and the electrode had to be carefully adjusted prior to each experiment. Secondly, only one picture could be taken during the first step of the bubble life because in these conditions the growth rate was very high and the bubble diameter was very small, lower than the optical resolution of the device.

3. Results

Two types of experimental result were obtained in this study. First, by using the repetitive growth of only one bubble on a microelectrode, the correlation between the bubble diameter and the induced overpotential was established. Second, the overpotential due to spheres of various sizes, placed on the electrode surface, was investigated.

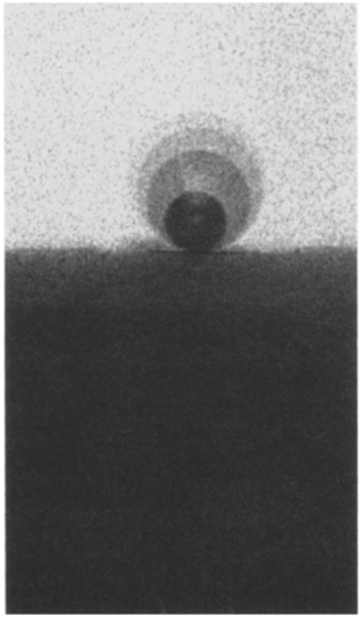

Fig. 3. Photograph of the sequential pictures of the bubble during its growth.

3.1. *Time evolution of the diameter of a bubble growing on a microelectrode and of the induced overpotential*

This study was carried out in 1 M NaOH on a 100 μm diameter platinum microelectrode where the repetitive formation of a single bubble of oxygen was observed under current control at I = 67 μA.

Figure 4 gives the time evolution of the bubble diameter (Fig. 4a) and the overpotential increment $\Delta V(t)$ (Fig. 4b). On curve a, the vertical bars show the estimation of the measurement errors. This plotting shows two successive evolution regimes. In the first the bubble radius changes as $t^{1/2}$, and in the second, when the bubble size exceeds the electrode size, the radius evolves as $t^{1/3}$. The change appears when the bubble diameter is larger than one and a half times the electrode diameter. Similarly, the overpotential regime changes at about the same time, passing from t to $t^{2/3}$.

In the first regime

$$\Delta V = k_1 t$$

and in the second (5)

$$\Delta V = k_2 t^{2/3}$$

These results are in agreement with the theoretical predictions. They show that in the first regime the growth is limited by the diffusion of the dissolved gas in the solution and in the second by the kinetics of gas production. The very first stage of growth has not been obtained as it is too fast and lasts less than 50 ms.

In Fig. 5 the overpotential increment $\Delta V(t)$ has been plotted versus the square of the bubble diameter. For both growth regimes $\Delta V(t)$ is proportional to the square of the bubble diameter

$$\Delta V \propto d_b^2 \quad (6)$$

In Fig. 6a the time evolution of the overpotential has been plotted for various electrolysis currents. Figure 6b shows that the coefficients k_1 and k_2 in Equation 5 vary approximately as $I^{5/3}$.

$$k_1, k_2 \propto I^{5/3} \quad (7)$$

This experimental result allows the coefficient β of

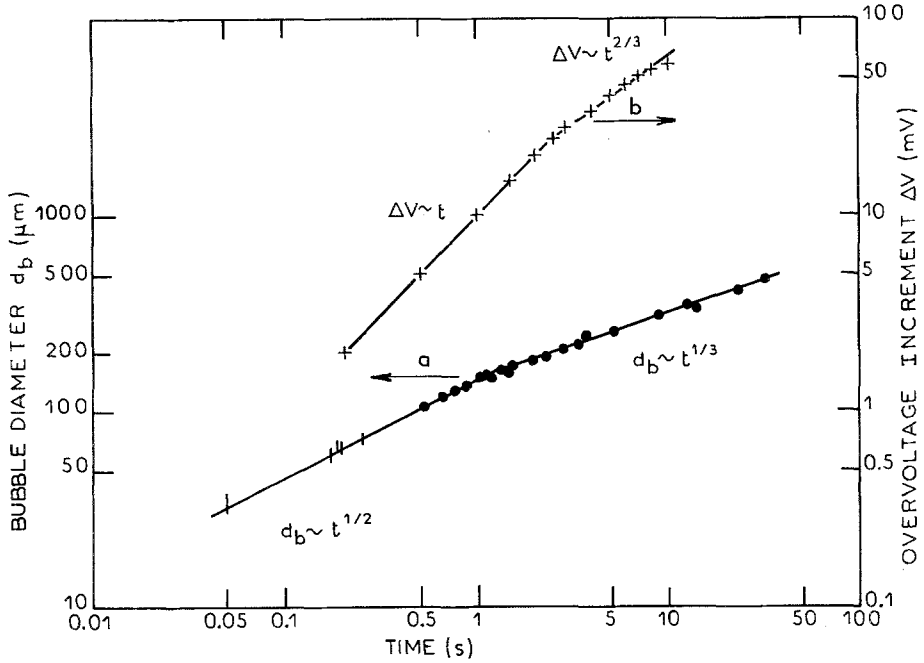

Fig. 4. Growth of an oxygen bubble on a microelectrode (d_e = 100 μm, I = 67 μA, 1 M NaOH). (a) Bubble diameter d_b; (b) overpotential increment ΔV due to the bubble.

the Scriven law (Equation 2) to be attained. For the regime controlled by diffusion, Equations 2 and 5 give

$$\Delta V = \frac{k_1}{16\beta^2 D} d_b^2 \tag{8}$$

and for the regime controlled by the electrolysis current, Equations 3 and 5 give

$$\Delta V = \frac{k_2}{4\left(\frac{3V_0 I}{4\pi nF}\right)^{2/3}} d_b^2 \tag{9}$$

The ratio $\Delta V/d_b^2$ is very close in the two growth regimes as shown in Fig. 5. Hence from Equations 8 and 9

$$\frac{k_1}{16\beta^2 D} = \frac{k_2}{4\left(\frac{3V_0 I}{4\pi nF}\right)^{2/3}} \tag{10}$$

By using Equation 7, it is shown that the Scriven coefficient, β, is proportional to $I^{1/3}$ which is in agreement with other authors [7, 17]. Equation 9 shows that

$$\Delta V \propto I^{\alpha} d_b^2 \tag{11}$$

where $\alpha = 1$. However, from the experimental point of view it is shown from Fig. 6a that α is slightly greater than 1.

3.2. *Identification of the overpotential due to a sphere on the electrode surface*

In this part, the origin of the overpotential (primary, secondary or tertiary potential distribution) has been investigated by measuring the impedance and the overpotential increment due to the presence of a sphere placed on the electrode centre which simulates

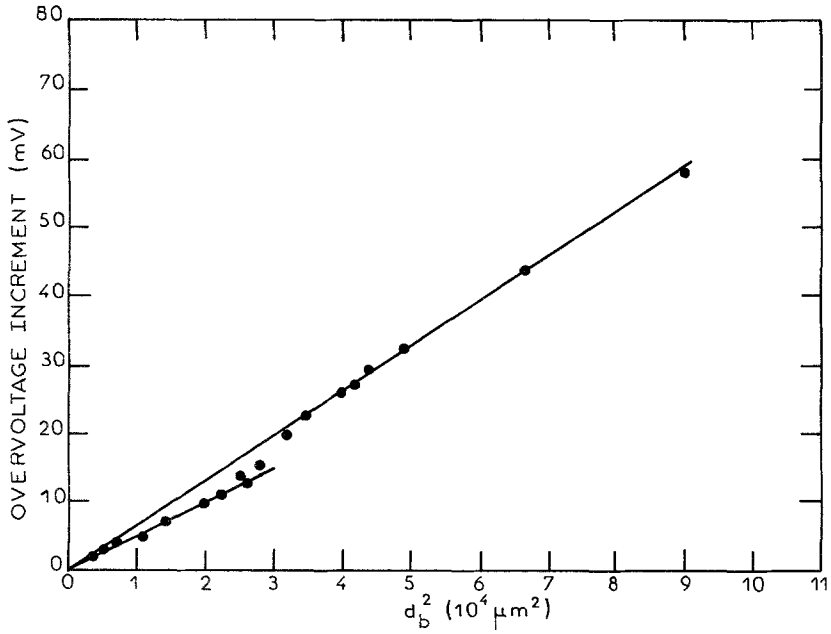

Fig. 5. Overpotential increment ΔV versus the square of the bubble diameter d_b^2 (same experimental conditions as Fig. 4).

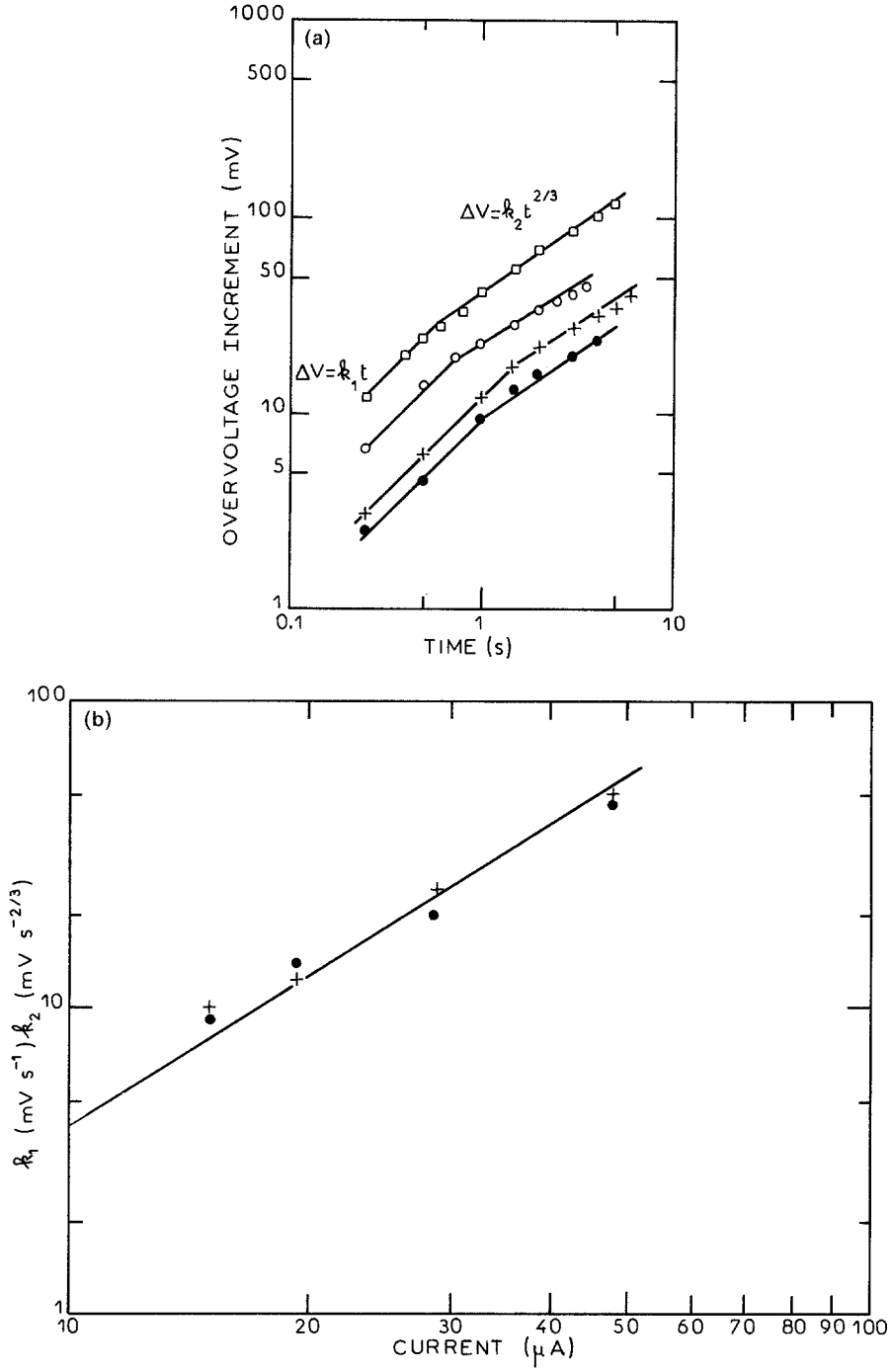

Fig. 6. (a) Time evolution of the overpotential due to the growth of an oxygen bubble on a microelectrode for various currents I: (●) 15.1; (+) 19.3; (○) 28.8; (□) 47.7 μA. (b) Variation of the coefficients k_1 and k_2 of Equation 5 (same experimental conditions as Fig. 4).

a 'frozen' bubble attached to the electrode. The impedance technique is quite appropriate for characterizing the potential distribution around the bubble. However, as this technique cannot be used on a growing bubble it is necessary to 'freeze' the bubble on the electrode by switching off the current.

3.2.1. Impedance variation due to a 'frozen' bubble. There are two types of limitation to this technique. First it is not possible to freeze large bubbles and, second, only the high frequency part of the impedance can be used as the low frequency part is controlled by the diffusion of the reactive species and, hence, the measured impedance is perturbed by the natural convection.

The increment of the electrolyte resistance, ΔR_e due to the presence of a bubble on the electrode is obtained from the shift of the high frequency limit of the real part of the impedance diagram plotted in the complex plane. The results obtained for a 1 mm diameter platinum electrode in sulphuric medium in the presence of hydrogen bubbles have been plotted in Fig. 7. They show that ΔR_e is proportional to the square of the bubble diameter.

$$\Delta R_e \propto d_b^2 \tag{12}$$

In addition, Fig. 7 shows that a sphere used in order to simulate the presence of a large 'frozen' bubble has the same influence on the electrolyte resistance incre-

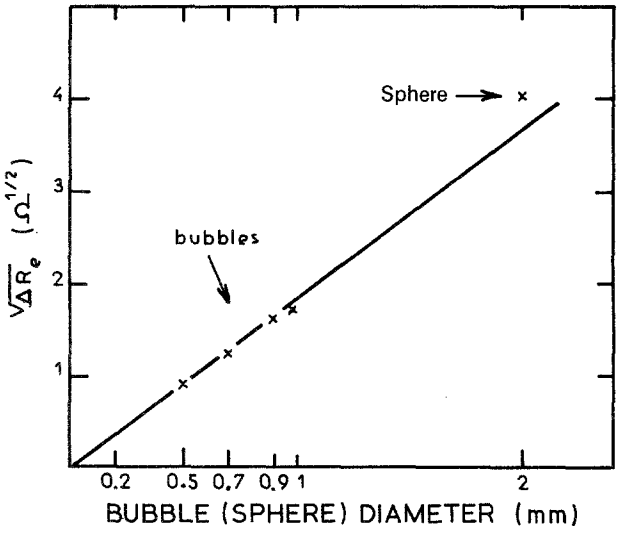

Fig. 7. Electrolyte resistance increment ΔR_e, obtained from impedance measurement, versus the diameter of a bubble or a sphere placed on a 1 mm diameter platinum disk electrode in sulphuric medium 1 M ($I = 0$).

ment as the real bubble, except for a slight deviation which could be due to a contact angle different from zero.

3.2.2. Impedance variation due to a sphere. This study was carried out on a 5 mm diameter iron disc electrode in 1 M H_2SO_4 electrolyte. In this electrochemical system, two processes occur simultaneously: iron dissolution and hydrogen production. In order to avoid the formation of hydrogen bubbles which could perturb the influence of the sphere on the electrode, the measurements have been performed with a slightly anodic polarization current (between 10 and 30 mA cm^{-2}) where the hydrogen production is negligible. In this domain the dissolution mechanism is well known and the impedance diagram (Fig. 8) shows three characteristic resistances: the charge transfer resistance, R_t, the polarization resistance, R_p (low frequency limit of the impedance) and the electrolyte resistance, R_e (high frequency limit of the impedance). When a sphere is placed on the electrode, the potential distribution is perturbed around the electrode leading to characteristic impedance changes: $R_t + \Delta R_t$, $R_p + \Delta R_p$ and $R_e + \Delta R_e$, as demonstrated by the impedance measurements (Fig. 8). The resistance increments ΔR_t, ΔR_p and ΔR_e have been plotted in

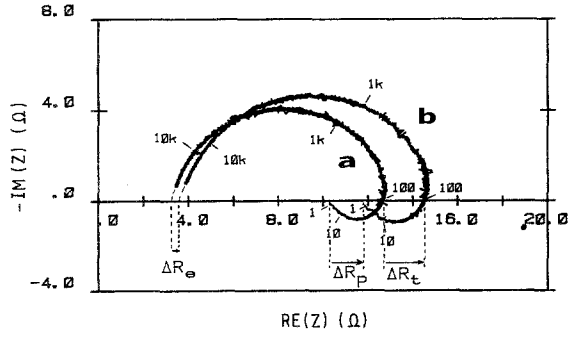

Fig. 8. Impedance diagrams measured on an iron disc electrode (Johnson Matthey, d_e = 5 mm, 1 M H_2SO_4). (a) Without sphere; (b) with a 3 mm diameter sphere placed on the surface centre.

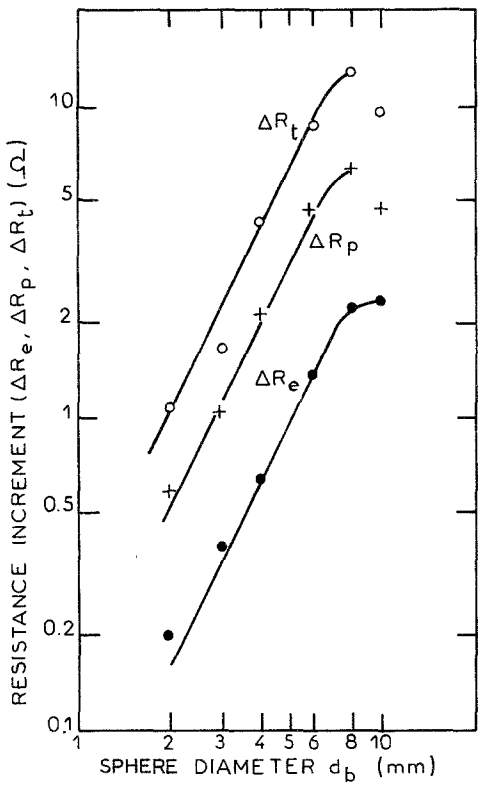

Fig. 9. Resistance increments ΔR_t, ΔR_p, ΔR_e versus the sphere diameter (same experimental conditions as Fig. 8).

Fig. 9 versus the sphere diameter. This shows that the resistance increments vary as d_b^2

$$\Delta R_t, \Delta R_p, \Delta R_e \propto d_b^2 \qquad (13)$$

except for spheres of large diameter (larger than the diameter of the electrode). This is in agreement with Equation 12 relative to the frozen bubbles.

In addition, the impedance diagram shows that in these experimental conditions there is no extra overpotential due to a concentration gradient as there is no diffusion impedance revealed by this experimental diagram (Fig. 8).

3.2.3. Overpotential due to a sphere. The overpotential was measured just after the sphere was placed in the centre of the disc electrode. The influence of the current and the electrode diameter was investigated. The experimental results were averaged over four experiments which gave a 1 mV resolution.

In Fig. 10a the overpotential increment ΔV has been plotted versus the diameter of the spheres on a 5 mm diameter disc electrode. This figure shows that the increment ΔV is proportional to the square of the diameter of the sphere as long as it does not exceed about twice that of the electrode

$$\Delta V \propto d_b^2 \qquad (14)$$

Figure 10b shows that the ratio $\Delta V/I$ is independent of the current I and that

$$\frac{\Delta V}{I} \propto d_b^2 \qquad (15)$$

In Fig. 11a the overpotential increment, ΔV, has been plotted for two electrodes of different diameters

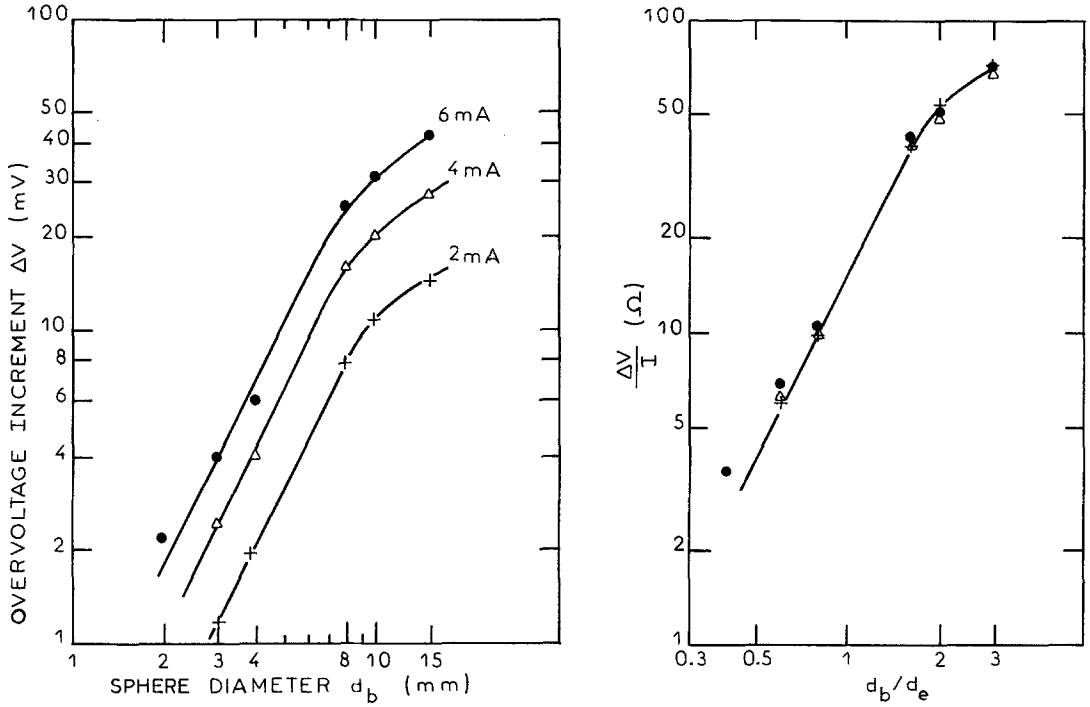

Fig. 10. (a) Influence of the electrolysis current on the overpotential increment due to a sphere placed on the electrode (same experimental conditions as Fig. 8). (b) Resistance increment $\Delta V/I$ versus the ratio of the diameter of the sphere over that of the electrode (same experimental conditions as Fig. 8).

for various electrolysis currents. This shows that, as previously, ΔV is proportional to the square of the sphere diameter (except when it is too large) and that, for a given sphere diameter and current, ΔV decreases when the electrode diameter increases.

Figure 11b shows that $\Delta V/I$ is proportional to the square of the ratio of the sphere diameter, d_b, over the electrode diameter, d_e, the proportionality factor being dependent on d_e.

$$\frac{\Delta V}{I} \propto \left(\frac{d_b}{d_e}\right)^2 \tag{16}$$

4. Discussion

Experimental results obtained here concern both the steady state and dynamic behaviour of the overpotential increment due to a bubble attached or growing on an electrode.

4.1. *Steady state overpotentials*

The resistance increments ΔR_e, ΔR_t and ΔR_p obtained from impedance measurements are proportional to d_b^2; therefore they can be considered as proportional to the projected surface of the bubble. Hence the experimental results can be interpreted by considering an equivalent total screening of only a part of the active surface of the electrode due to the sphere or the bubble where the current is supposed to be zero, whereas the current is supposed to be uniform outside the screened surface.

To the polarization resistance, R_p, which is

$$R_p = \frac{R_{p0}}{S} \tag{17}$$

where R_{p0} is the polarization resistance per surface unit without a bubble on the electrode and S is the electrode area, there corresponds an equivalent screened surface given by

$$\frac{\Delta S_p}{S} = -\frac{\Delta R_p}{R_p} \tag{18}$$

for small values of ΔS_p and ΔR_p.

In the framework of the screened surface approximation the overpotential of an electrode immersed in an electrolyte can be written

$$V = R_e I + f\left(\frac{I}{S}\right) \tag{19}$$

Under current control the addition of a sphere, or of a bubble, on the electrode surface gives rise to an increment of R_e, R_p and V such that

$$\Delta V = \Delta R_e I + \frac{\partial f}{\partial (I/S)}\left(-\frac{I\Delta S_p}{S^2}\right) \tag{20}$$

$$= \Delta R_e I + R_{p0}\left(-\frac{I\Delta S_p}{S^2}\right) \tag{21}$$

$$= \Delta R_e I + R_p\left(-\frac{I\Delta S_p}{S}\right) \tag{22}$$

and by using Equation 18

$$\Delta V = \Delta R_e I + \Delta R_p I \tag{23}$$

In this derivation, which is valid for non-linear current–voltage relationships, Equation 23 is valid only for small changes, ΔS_p, ΔR_e, ΔR_p and ΔV, i.e. for small spheres or bubbles. However, in the experimental results given here this type of relationship seems to be valid up to sphere diameters larger than the electrode diameter. In the experimental conditions chosen (iron

electrode in sulphuric medium close to the corrosion potential) the current–overpotential relationship is nearly linear and can be approximated by

$$\eta_t = (R_e + R_p)I \tag{24}$$

In this case, whatever the size of the sphere which gives rise to resistance increments ΔR_e and ΔR_p,

$$\Delta V = \Delta\eta_t = \eta_t(\text{with sphere}) - \eta_t(\text{without sphere}) \tag{25}$$

$$= (R_e + \Delta R_e + R_p + \Delta R_p)I - (R_e + R_p)I \tag{26}$$

$$= (\Delta R_e + \Delta R_p)I$$

Therefore in a linear region Equation 23 is valid whatever the values of the quantities ΔR_e and ΔR_p, i.e. whatever the size of the sphere or bubble.

The equivalent screened surface, ΔS_p, can be estimated by using Equation 18 and the data of Fig. 9 and by defining

$$|\Delta S_p| = \alpha_p \frac{\pi}{4} d_b^2 \tag{27}$$

as $R_p = 10.5\,\Omega$, $S = 0.2\,\text{cm}^2$, one has $\alpha_p = 0.3$.

The presence of the sphere on the electrode leads to a rearrangement of the current lines which gives an equivalent screening effect of 30% of the projected surface of the sphere.

From Equations 18 and 27 the relative change of R_p can be evaluated

$$\frac{\Delta R_p}{R_p} = \alpha_p \left(\frac{d_b}{d_e}\right)^2 \tag{28}$$

For the electrolyte resistance increment, ΔR_e, it has been shown, on a theoretical basis [18] in the case of a ring disc electrode, that ΔR_e is proportional to d_d^3, where d_d is the diameter of an insulating disc. On the other hand, in the case of an infinite electrode, it has been shown that ΔR_e is also proportional to d_b^3, where d_b is the diameter of the bubble [19]. The present experimental results are not in agreement with these theoretical predictions as ΔR_e is proportional to d_b^2.

As ΔR_e and ΔR_p behave in a similar way, i.e. a small bubble or sphere put on a small electrode has the same relative effect on R_e and R_p as a large bubble or sphere on a large electrode (with the same d_b/d_e ratio), the same relationships as Equations 18, 27 and 28 can be assumed for the electrolyte resistance increment. Hence

$$\frac{\Delta S_e}{S} = -\frac{\Delta R_e}{R_e} \tag{29}$$

$$|\Delta S_e| = \alpha_e \pi \frac{d_b^2}{4} \tag{30}$$

$$\frac{\Delta R_e}{R_e} = \alpha_e \left(\frac{d_b}{d_e}\right)^2 \tag{31}$$

where α_e, like α_p, is independent of d_e and d_b.

As for a disc electrode of diameter d_e, R_e and R_p can be written in the form

$$R_e = \frac{R_{e0}}{d_e} \tag{32}$$

$$R_p = \frac{4R_{p0}}{\pi d_e^2} \text{ from Equation 17} \tag{33}$$

Then

$$\Delta R_e = \alpha_e R_{e0} \frac{d_b^2}{d_e^3} \tag{34}$$

and

$$\Delta R_p = \frac{4}{\pi} \alpha_p R_{p0} \frac{d_b^2}{d_e^4} \tag{35}$$

The total overpotential increment due to the presence of a sphere or a bubble is therefore

$$\Delta V = I\left(\alpha_e R_{e0} \frac{d_b^2}{d_e^3} + \frac{4}{\pi} \alpha_p R_{p0} \frac{d_b^2}{d_e^4}\right) \tag{36}$$

i.e.

$$\Delta V = I\left(\alpha_e R_{e0} \frac{1}{d_e} + \frac{4}{\pi} \alpha_p R_{p0} \frac{1}{d_e^2}\right)\left(\frac{d_b}{d_e}\right)^2 \tag{37}$$

Equation 37 explains why, for the same d_b/d_e ratio, the experimental overpotential increment is lower for a larger electrode (see Fig. 11b).

The ratio of the overpotential increments related to the primary potential distribution $\Delta V_{ohm} = \Delta R_e I$ and to the secondary potential distribution $\Delta V_a = \Delta R_p I$ can be estimated

$$\frac{\Delta V_a}{\Delta V_{ohm}} = \frac{\Delta R_p}{\Delta R_e} \tag{38}$$

$$\frac{\Delta V_a}{\Delta V_{ohm}} = \frac{4\alpha_p R_{p0}}{\pi \alpha_e R_{e0} d_e} \tag{39}$$

As an example, this ratio is equal to 3 in the case of the experimental conditions of Fig. 9. Equation 39 shows that, when the size of the electrode increases, the overpotential will be predominantly determined by the primary potential distribution, i.e. ohmic drop. This is also true, from Equation 38, when R_p decreases, which is often the case when the electrolysis current increases. This behaviour is similar to that of a non-screened electrode.

On the other hand, from the data depicted in Fig. 9 and using Equation 23, one has

$$\frac{\Delta V}{I} = \Delta R_e \left(1 + \frac{\Delta R_p}{\Delta R_e}\right) \tag{40}$$

$$\frac{\Delta V}{I} = \Delta R_e \left(1 + \frac{3}{d_e}\right) \tag{41}$$

where d_e unit is mm.

Hence for two electrodes of diameters d_e and d_e' the ratio of the overpotential increments, for the same d_b/d_e ratio, is

$$r = \frac{\left(\frac{\Delta V}{I}\right)_{d_e}}{\left(\frac{\Delta V}{I}\right)_{d_e'}} \tag{42}$$

$$= \frac{\frac{1}{d_e}\left(1 + \frac{3}{d_e}\right)}{\frac{1}{d_e'}\left(1 + \frac{3}{d_e'}\right)} \tag{43}$$

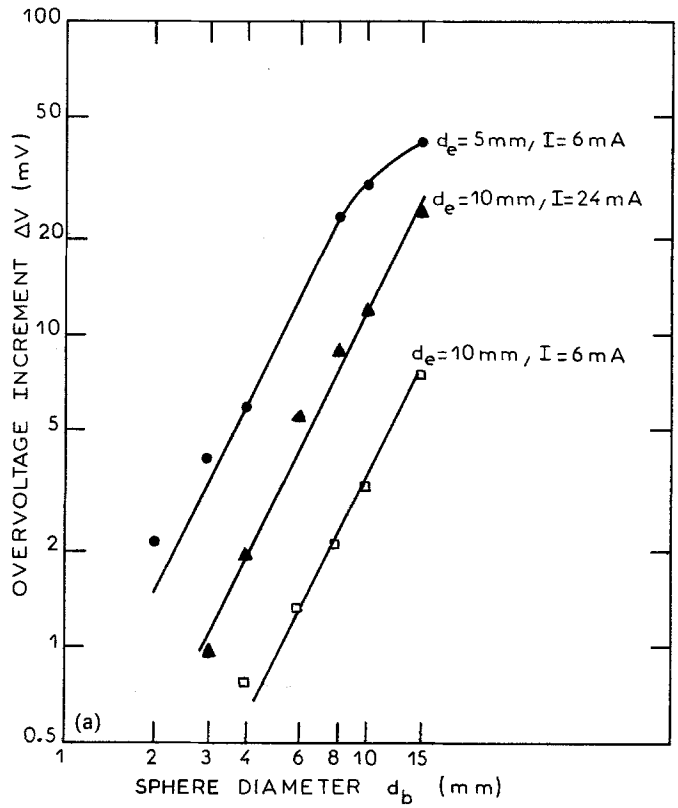

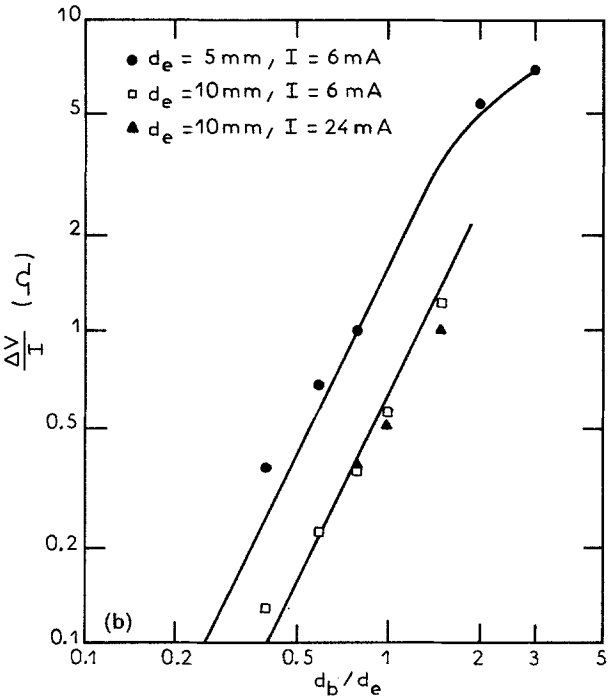

Fig. 11. (a) Influence of the electrode diameter d_e on the overpotential increment due to a sphere placed on the electrode (same experimental conditions as Fig. 8). (b) Resistance increment $\Delta V/I$ versus the ratio d_b/d_e.

For $d_e = 5$mm and $d'_e = 10$mm, $r = 2.5$. The data plotted in Fig. 11b give $r = 2.9$. The good agreement between experimental and theoretical results supports the various assumptions used in this study.

4.2. *Dynamic overpotential increment due to a growing bubble*

It will be considered that the variations of the resistance increments ΔR_e, ΔR_p and ΔR_t are due to the variations of the equivalent screened surfaces ΔS_e, ΔS_p, ΔS_t due to a bubble of radius r_b. Thus

$$\Delta S_j = \alpha_j \pi r_b^2 \qquad (44)$$

where the parameter α_j depends upon the considered resistance (i.e. depends upon the frequency). In order to calculate the time evolution of the overpotential increment $\Delta V(t)$ due to the bubble growth it is assumed that this bubble growth leads to a decrease of the electrode active surface. This surface change, ΔS, produces a variation of all the parameters depending on the surface which characterize the kinetics of the system (R_t, R_p, C. . .). In this approach therefore, it will be considered that all the screened surfaces ΔS_e, ΔS_p, ΔS_t are equal to ΔS.

The electrode is polarized at a constant current I. At time $t = 0$, a bubble is born and begins to grow. Due

to the screening effect the electrode active surface changes as

$$S = S_i(1 - st) \quad (45)$$

where S_i is the surface at time $t = 0$, without the bubble. The surface change $\Delta S = -S_i st$ is proportional to the time insofar as on the one hand

$$\Delta S = \alpha \pi r_b^2 \quad (46)$$

where α is a constant and on the other hand the radius of the bubble r_b changes as $\sqrt{t}$ when the growth is limited by the dissolved gas diffusion. In these conditions it can be shown for various reaction mechanisms on the electrode (see Appendix) that the overpotential increment is the sum of two terms proportional to time t, one term due to the ohmic effect and the other to the kinetic effect.

$$\Delta V(t) = IR_{pi} st + IR_{ei} st \quad (47)$$

where R_{pi} and R_{ei} are the polarization and the electrolyte resistances in the absence of the bubble.

By using Equations 18 and 29

$$\frac{\Delta R_p}{R_{pi}} = -\frac{\Delta S}{S_i} = -st \quad (48)$$

$$\frac{\Delta R_e}{R_{ei}} = -\frac{\Delta S}{S_i} = -st \quad (49)$$

Equation 23 is found again from Equation 47.

The linear relationship with time (Equation 47) of the overpotential variation is in agreement with the experimental result obtained on a microelectrode in the case of dissolved-gas-diffusion-controlled growth (first regime in Fig. 2). This regime is often experimentally found on macroelectrodes (larger than a few mm) as in this case the sizes of the bubbles are lower than the electrode size and, therefore, their growths are diffusion controlled (except when bubble coalescence occurs).

When several bubbles are simultaneously growing on the surface, if the number of bubbles remains low, or the bubbles are small compared to the electrode size, the total surface screened by the bubbles remains low compared to the electrode surface and can be calculated as the sum of the surfaces screened by each bubble: the elementary overpotential increments of each bubble simply add. Hence the overpotential increment due to the growth of a small number of bubbles, or bubbles of small diameter ($\Delta S \ll S_i$) increases linearly with time. When the number of bubbles becomes large, the perturbations of the potential due to each bubble interact and induce a significant increase of the overpotential, as shown by Dukovic and Tobias [13].

From the experimental point of view, this linear time variation of the overpotential has already been found in the case of iron dissolution close to the corrosion potential in sulphuric acid where a few hydrogen bubbles grow slowly on the electrode [15].

5. Conclusion

The total overpotential measured on a gas-evolving electrode fluctuates because of the continuous change of the number and size of bubbles on the electrode. In order to understand the origin of the overpotential fluctuations (ohmic and/or activation and/or concentration effects), gas evolution has been studied in this paper for only one bubble on the electrode and for a glass sphere simulating a frozen bubble.

The measured total overpotential has been characterized under current control by the increments of the electrolyte resistance and the polarization resistance, which have been evaluated from impedance measurements. The ratio of these increments allows the type of control (ohmic, activation and, in other conditions, concentration) to be assessed.

In the experimental conditions used (hydrogen evolution during iron dissolution), the various components of the total overpotential are interpreted as the result of a screening effect due to the bubble or the sphere which masks a part of the active surface of the electrode. By studying this screening effect, which is related to the potential distribution and hence is frequency dependent, a relationship has been obtained, for a given electrode diameter, between the bubble or the sphere diameter and the induced overpotential increment.

For a gas-evolving electrode, this relationship allows some parameters characteristic of the gas evolution, usually determined from optical techniques, to be derived from the analysis of the fluctuations of an electrical quantity, the electrode overpotential. The derivation of these parameters, such as the mean number of bubbles evolved per time unit, the bubble detachment mean radius and the gas evolution efficiency (i.e. the amount of produced molecular gas evolved under bubble form) is illustrated in [14] for gas evolution in water electrolysis.

Two more results are shown in this paper. First, for gas evolution on macroelectrodes (large diameter electrodes) it can be concluded that, as the maximum diameter reached by the bubbles is small compared to the size of the electrode, the observable growth of the bubble is controlled by the transport, by diffusion of the dissolved molecular gas (if the coalescence phenomenon is not taken into account) and not by the kinetics of the production of the dissolved gas. Second, if the bubble is supposed to grow under molecular gas diffusion control and the overpotential is due to a screening effect, a theoretical calculation has shown that the overpotential changes linearly with time, which agrees with experimental findings [15, 21].

Appendix: Derivation of the time evolution of the overpotential due to the growth of a bubble

When the bubble grows on the electrode surface under current control, the total current which flows through the electrode is constant ($I = I_0$). It is the sum of the faradaic current, I_F, and the charging curent, dQ/dt, of the double layer capacity, C.

$$I_0 = I_F + \frac{dQ}{dt} \quad (A1)$$

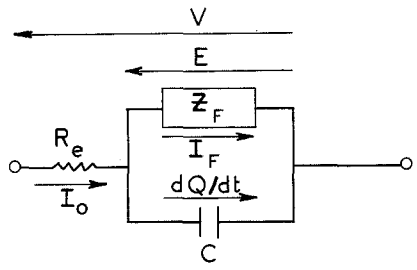

Fig. 12. Equivalent circuit used for the derivation of the overpotential time evolution.

The charge, Q, of the double layer is equal to

$$Q = C(E - E_z) \tag{A2}$$

where E_z is the zero charge potential and E the electrode potential (see Fig. 12). The measured potential, V, takes into account the ohmic drop.

$$V = E + R_e I_0 \tag{A3}$$

Hence from Equation A1 and using Equation A2

$$I_0 = I_F + (E - E_z)\frac{dC}{dt} + C\frac{dE}{dt} \tag{A4}$$

where the double layer capacity, C, is surface dependent

$$C = C_0 S \tag{A5}$$

Two types of reaction mechanism have been investigated: a simple redox process and a two-step charge transfer process [20]. These mechanisms can be either the reaction mechanism at the origin of the molecular gas production, or a parallel reaction mechanism which reveals the gas bubble evolution through the electrode surface change.

Redox reaction mechanism

$$A + e \underset{k_b}{\overset{k_f}{\rightleftharpoons}} B$$

In order to simplify the calculation presentation no limitation by mass transport is assumed so that concentrations of species A and B (C_A and C_B) are constant. Then

$$I_F = FS(k_b C_B - k_f C_A) \tag{A6}$$

where the reaction rates, k_b and k_f, are assumed to follow a Tafel law

$$\begin{aligned} k_f &= k_{f0} \exp(-b_f E) \\ k_b &= k_{b0} \exp(b_b E) \end{aligned} \tag{A7}$$

The time evolution of the potential, E, is governed by Equation A4 which gives, using Equation A6

$$C\frac{dE}{dt} + (E - E_z)\frac{dC}{dt} + FS(k_b C_B - k_f C_A) = I_0 \tag{A8}$$

For small changes, ΔE, about the polarization point, E_0, due to the surface change, ΔS, one has

$$\begin{aligned} I_0 = {} & C\frac{d\Delta E}{dt} + \Delta E\frac{dC}{dt} + (E_0 - E_z)\frac{dC}{dt} \\ & + FS(k_b C_B - k_f C_A) + FS(k_b b_b C_B \\ & + k_f b_f C_A)\Delta E \end{aligned} \tag{A9}$$

where k_b and k_f are hereafter the values of the rate constants at potential E_0.

At time $t = 0$, the faradaic current, I_F, is equal to I_0

$$I_0 = FS_i(k_b C_B - k_f C_A) \tag{A10}$$

From Equations A9, A10 and 45, one obtains the differential equation which governs the ΔE time evolution

$$\begin{aligned} & C\frac{d\Delta E}{dt} + \Delta E\left(\frac{dC}{dt} + \frac{1 - st}{R_{ti}}\right) \\ & + (E_0 - E_z)\frac{dC}{dt} - stI_0 = 0 \end{aligned} \tag{A11}$$

where

$$\frac{1}{R_{ti}} = \frac{\Delta I_F}{\Delta E} = FS_i(k_b b_b C_B + k_f b_f C_A) \tag{A12}$$

is the charge transfer resistance at potential, E_0, before bubble growth.

The derivative dC/dt is a constant given by Equations A5 and 45

$$\frac{dC}{dt} = -C_i s \tag{A13}$$

where C_i is the double layer capacity before bubble growth ($C_i = C_0 S_i$).

The integration of Equation A11 with initial condition $\Delta E(0) = 0$ leads to

$$\begin{aligned} \Delta E(t) = {} & \frac{s}{1 - st}\{(E_0 - E_z - I_0 R_{ti})R_{ti}C_i \\ & \times [1 - \exp(-t/R_{ti}C_i)] + I_0 R_{ti} t\} \end{aligned} \tag{A14}$$

After a short transient regime ($R_{ti}C_i \simeq 1$ ms, for data of Fig. 8) $\Delta E(t)$ varies linearly with time insofar as the surface change due to the bubble is small ($st \ll 1$).

$$\begin{aligned} \Delta E(t) = {} & I_0 R_{ti} st + (E_0 - E_z)R_{ti}C_i s^2 t \\ & + (E_0 - E_z)R_{ti}C_i s \end{aligned} \tag{A15}$$

when I_0 is different from zero and $R_{ti}C_i$ is low.

$$\Delta E(t) = I_0 R_{ti} st \tag{A16}$$

If the ohmic drop is taken into account, the total overpotential increment $\Delta V(t)$ is given by (from linearization of Equation A3)

$$\Delta V(t) = I_0 R_{ti} st + \Delta R_e(t) I_0 \tag{A17}$$

or with Equations 29 and 45

$$\Delta V(t) = I_0 R_{ti} st + I_0 R_{ei} st \tag{A18}$$

Two-step charge transfer

The same derivation has been carried out in the case of a two-step charge transfer [20, 21] which is a simplified model of iron dissolution in sulphuric acid close to the corrosion potential.

It has been found that

$$\Delta V(t) = I_0 R_{pi} st + I_0 R_{ei} st$$

which generalizes Equation A18 when the polarization resistance R_p is different from the charge transfer resistance R_t.

References

[1] S. Shibata, *Electrochim. Acta* **23** (1978) 619.
[2] S. Shibata, *Bull. Chem. Soc. Japan* **33** (1960) 1635.
[3] H. Vogt, *Electrochim. Acta* **29** (1984) 167.
[4] H. Vogt, *Electrochim. Acta* **25** (1980) 527.
[5] Lord Rayleigh, *Phil. Mag.* **34** (1917) 94.
[6] D. E. Westerheide and J. W. Westwater, *AIChE J.* **7** (1961) 357.
[7] N. P. Brandon and G. H. Kelsall, *J. Appl. Electrochem.* **15** (1985) 475.
[8] L. E. Scriven, *Chem. Eng. Sci.* **10** (1959) 1.
[9] S. Van Stralen, R. De Jonge and H. Verhaart, in 'Boiling Phenomena', Vol. 1 (edited by S. Van Stralen and R. Cole), McGraw Hill, New York (1979) Ch. VI.
[10] R. Darby and M. Haque, *Chem. Eng. Sci.* **28** (1973) 1129.
[11] K. J. Vetter, 'Electrochemical Kinetics, Theoretical and Experimental aspects' (edited by S. Brückenstein and B. Howard), Academic Press, New York (1967).
[12] J. A. Leistra and P. J. Sides, *J. Electrochem. Soc.* **134** (1987) 2442.
[13] J. Dukovic and C. W. Tobias, *J. Electrochem. Soc.* **134** (1987) 331.
[14] C. Gabrielli, F. Huet, M. Keddam and A. Sahar, *J. Appl. Electrochem* **19** (1989) 683.
[15] C. Gabrielli, F. Huet and M. Keddam, *J. Appl. Electrochem.* **15** (1985) 503.
[16] C. Gabrielli, F. Huet, M. Keddam and J. F. Lizee, *J. Electroanal. Chem.* **138** (1982) 201.
[17] J. P. Glas and J. W. Westwater, *Int. J. Heat Mass Transfer* 7 (1964) 1427.
[18] J. J. Miksis and J. Newman, *J. Electrochem. Soc.* **123** (1976) 1030.
[19] P. J. Sides and C. W. Tobias, *J. Electrochem. Soc.* **127** (1980) 288.
[20] A. Sahar, PhD Thesis, Université de Paris IV (1988).
[21] C. Gabrielli, F. Huet, M. Keddam and A. Macias, to be published.